Dependence of Ion-Implant-Induced LBIC Novel Characteristic on Excitation Intensity for Long-Wavelength HgCdTe-Based Photovoltaic Infrared Detector Pixel Arrays

Wei-Da Hu, Xiao-Shuang Chen, Zhen-Hua Ye, A-Li Feng, Fei Yin, Bo Zhang, Lei Liao, and Wei Lu

***Abstract*—In this paper, experimental results of laser-irradiance-dependent polarity inversion of laser beam induced current (LBIC) for As-doped long-wavelength HgCdTe pixel arrays grown on CdZnTe are reported. Models for the ion-implant-induced junction transformation are proposed, and demonstrated using numerical simulations. The novel trap-related p-n junction transformation induced by ion implantation is observed under typical laser irradiances for low temperature. The implantation-induced traps and Hg interstitial diffusion are key factors for inducing the LBIC coupling, polarity reversion, and junction broadening at different laser irradiances. The trap type, trap density, and junction configuration are extracted from the measured experiment data. The results provide the near room-temperature HgCdTe photovoltaic detector with a reliable reference on the junction reversion and broadening around implanted regions, as well as controlling the n-on-p junction formation for very long wavelength HgCdTe infrared detector pixels.**

***Index Terms*—Laser beam induced current, HgCdTe long wave infrared detector, junction transformation, device simulation.**

I. Introduction

DUE TO tunable absorption wavelengths, high quantum efficiency, and a wide operating temperature range, HgCdTe-based photodetectors are the promising devices of choice for many infrared thermal imaging systems [1]–[3]. Currently, typical HgCdTe infrared focal plane array (IRFPA) photodetectors operating at cryogenic temperatures are based on the n^+-on-p junction [4]–[7]. While molecular beam epitaxy and liquid phase epitaxy techniques have been extensively used in fabrication of HgCdTe films for many years, long wavelength HgCdTe IRFPAs still suffer severely from temperature and photo activated defects and nonuniformities in the performance of individual elements [8]–[11] due to the very small band gap and complex doping behavior for the p-n junction. Device fabrication yield for long wavelength HgCdTe IRFPAs is very low, typically less than 10% for large 2-D arrays, while the yields of Si-based CMOS and GaN-based LED are usually more than 90% and 80%, respectively [12]. The common junction profiles for the typical photovoltaic infrared detector are $n^+/n^-/p$ or $n^+/p^-/p$ according to the impurity background type along the junction [13]. Generally, $n^+/n^-/p$ is the preferred junction profile because the junctions can be formed away from the ion-implant-induced damage region and the junction depth can be controlled [13]. However, there are few convenient techniques that can quickly and nondestructively measure the junction profile of each pixel for an HgCdTe infrared focal plane array. Recently, laser beam induced current (LBIC) imaging has been used in determining the junction formation [14]–[17], and has been proven to be an effective method to detect the junction profiles of HgCdTe pixels for long wavelength infrared focal plane arrays. LBIC imaging can provide spatially resolved information about electrically active defects and localized nonuniformities in HgCdTe materials and devices used for infrared photovoltaic arrays [17]–[19].

However, analysis of LBIC measurements of HgCdTe-based photovoltaic detectors has been acknowledged to be a difficult task because of the large number of factors influencing the LBIC signal [18]–[20]. These factors include the junction type conversion at specific temperatures, ion implantation induced damage to the semiconductor materials, and mixed conduction near room temperature. Additionally, unique characteristic parameters of semiconductor material properties including the minority carrier lifetimes and diffusion lengths in vicinity of the p-n junction, and other nonideal effects such as surface recombination and localized leakage also influence the LBIC signal. The temperature and laser beam property dependence of LBIC imaging on mid-wavelength Hg-vacancy doped HgCdTe p-n junctions has been described by Redfern *et al*. [21], [22], who illustrated that a peak-to-peak LBIC signal would reach saturation under low temperature and high laser beam intensity conditions. Ion implantation of boron is usually used to create n^+-on-p photovoltaic detector in vacancy-doped or As-doped HgCdTe. In the n^+ region, the native point defects and complexes most likely trapped on extended defects form the electrical profile of a

Manuscript received November 30, 2012; revised March 30, 2013; accepted April 8, 2013. This work was supported in part by the State Key Program for Basic Research of China under Grants 2013CB632705 and 2011CB925604, the National Natural Science Foundation of China under Grants 11274331, 10990104, 61006090, and 61290301, the Aviation Science Fund under Grant 20110190001, and Shanghai Rising-Star Program.

W.-D. Hu, X.-S. Chen, Z.-H. Ye, A.-L. Feng, F. Yin, B. Zhang, and W. Lu are with the National Laboratory for Infrared Physics, Shanghai Institute of Technical Physics, Chinese Academy of Sciences, Shanghai 200083, China (e-mail: wdhu@mail.sitp.ac.cn; xschen@mail.sitp.ac.cn).

L. Liao is with the Department of Physics and Key Laboratory of Artificial Micro- and Nano-structures of Ministry of Education, Wuhan University, Wuhan 430072, China.

Color versions of one or more of the figures in this paper are available online at http://ieeexplore.ieee.org.

Digital Object Identifier 10.1109/JSTQE.2013.2257992

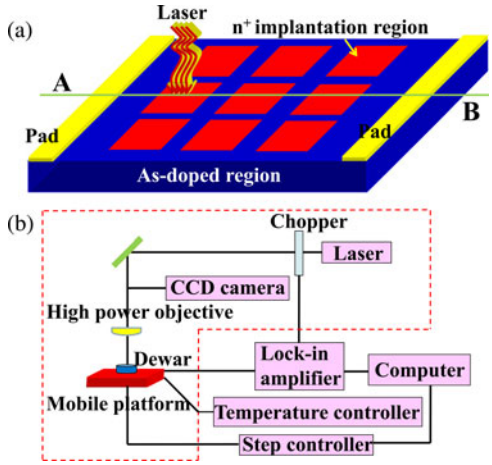

Fig. 1. (a) Schematic of HgCdTe infrared detector pixel arrays. The pixel size of the detector pixel array is 200 μm with the array format of 256 $\times$ 256 pixels. The ion-implantation window is 50 μm $\times$ 50 μm. (b) Experimental setup for measurement of laser beam induced current.

p-n junction. Those defects and complexes are induced by the interaction of the implant-induced strain and of structural defects in the material [13], [23]. The ion implantation damage could potentially induce a deformation of the LBIC. Therefore, a typical experimental setup and robust model are definitely required that can analyze the implant-induced junction transformation and extract the corresponding characteristic parameters for long-wavelength HgCdTe infrared detector arrays.

In this paper, experimental results of laser-irradiance-dependent junction transformation for long-wavelength HgCdTe pixel arrays grown on CdZnTe are reported. The ion-implant-induced p-n junction has been observed for the first time in the long-wavelength HgCdTe pixel arrays. Both the experimental and theoretical results show that laser irradiance has a significant effect upon LBIC imaging. Models of the ion-implantation-induced junction transformation are proposed. By using the numerical simulation, the trap type, trap density, and trap-related junction width of ion-implant-induced p-n junction in the detector pixel arrays are obtained.

II. Device Description and Experimental Setup

In preparation for the experiment liquid phase, epitaxially grown, As-doped, p-type $Hg_{1-x}Cd_xTe$ ($x \approx 0.224$) layers were grown on CdZnTe substrates. Then, n-on-p diodes with an ion-implantation size of $W \approx 50$ μm were fabricated on the p-type HgCdTe layers through B^+ ion implantation. The boron ion implantation process was carried out using an IM200 implanter with implant energy of 110 keV and an implant dosage of 1×10^{14} cm^{-2} at room temperature. After the implantation process and removal of photoresist, a ZnS film with a thickness of 240 nm was evaporated onto the device as a passivation layer. The remote contacts were deposited with gold on either side of the n-on-p junctions in preparation for LBIC measurements. The pixel size of the detector pixel array is 200 μm with the array format of 256 $\times$ 256 pixels. The schematic of HgCdTe infrared detector pixel arrays is shown in Fig. 1(a). An n^+-on-p abrupt junction is expected with a doping profile of $N_d \approx 1 \times 10^{17}$ cm^{-3}, $N_a \approx 1 \times 10^{16}$ cm^{-3}, and an n^+ heavy-doping area of 50 μm $\times$ 50 μm for the HgCdTe pixel arrays. According to the electrical characterization data of the diodes, R0A is approximately 2.5 Ω·cm^2 at 77 K indicating that the detector pixel array is quite normal. The LBIC measurements were undertaken in a cryostat with the sample in a chip carrier for bonding the remote contacts. A laser microscope was used as the source of He-Ne laser irradiance at a wavelength of 0.63 μm. The laser beam focuses a 1.4$\sim$1.6 μm diameter spot on the sample resulting in an optical power density of approximately $10^3 \sim 10^5$ W/cm^2. The beam then steps across the sample in the horizontal direction. The induced current is recorded by a SR830 DSP lock-in amplifier as a function of x--y scanning coordinates to provide a spatial LBIC map, shown in Fig. 1(b).

III. Analysis Model and Simulations

Steady-state numerical simulations are performed using Sentaurus Device (Synopsys 2010), a commercial package by Synopsys. For plain drift-diffusion simulation the well-known Poisson and continuity equations are used [2], [24], [25]. The steady-state continuity equations for electrons and holes are

$$\frac{1}{q}\nabla \vec{J}_n + (G - R) = 0 \tag{1}$$

$$\frac{1}{q}\nabla \vec{J}_p - (G - R) = 0 \tag{2}$$

and Poisson's equation is

$$\nabla^2 \psi = -\frac{q}{\varepsilon_0 \varepsilon}(\Gamma + p - n) - \frac{1}{\varepsilon}\nabla\psi\nabla\varepsilon. \tag{3}$$

Here, R is the carrier recombination rate, and G is the carrier generation rate. The electron and hole current densities, which can be expressed as a sum of diffusion and drift components, are listed as follows:

$$\vec{J}_n = qn\mu_n \vec{E}_n + qD_n \nabla n \tag{4}$$

$$\vec{J}_p = qp\mu_p \vec{E}_p - qD_p \nabla p. \tag{5}$$

Equations (4) and (5) can simply be expressed as a function of the Fermi quasi-level Φ_e and Φ_h during the numerical simulations

$$\vec{J}_n = qn\mu_n \nabla \Phi_e \tag{6}$$

$$\vec{J}_p = qn\mu_p \nabla \Phi_h \tag{7}$$

where J_n and J_p are the electron and hole current densities, respectively, and n and p are the concentration for the electron and hole, respectively. Γ is the effective doping density defined as the net value of the donor and acceptor doping densities. q is the electron charge, $\varepsilon_0\varepsilon$ is the permittivity of the semiconductors, and Ψ is the electrostatic potential. D_n and D_p are the electron and hole diffusion coefficients, and E_n and E_p are the electron and hole effective electric fields, respectively. μ_n and μ_p, the

mobility for electrons and holes, are [26]

$$\mu_n = 9 \times 10^4 \left(\frac{0.2}{x}\right)^{7.5} T^{-2(0.2/x)^{0.6}} \tag{8}$$

$$\mu_p = 0.01\mu_n. \tag{9}$$

In the numerical simulations, the optical generation rate can be expressed as [27]–[29]

$$G^{opt}(z) = J(x, y, z_0) \cdot \alpha(\lambda, z) \cdot \exp\left[-\left|\int_{z_0}^{z} \alpha(\lambda, z)dz\right|\right] \tag{10}$$

where λ is the wavelength, $J(x, y, z_0)$ is the optical beam spatial variation of intensity over a window where rays enter the device, z_0 is the position along the ray where absorption begins, and $\alpha(\lambda, z)$ is the absorption coefficient along the line. The absorption coefficient is calculated according to the following fitting equations [30]:

$$\alpha(E_{ph}) = \begin{cases} \alpha_1 \exp((E_{ph} - E_1)/E_2), E_{ph} < E_1 \\ \alpha_1 + \alpha_2((E_{ph} - E_1)/E_2)^P, E_{ph} \geq E_1 \end{cases} \tag{11}$$

where E_{ph} is the photon energy, $\alpha_1, \alpha_2, E_1, E_2$, and P are the model parameters of HgCdTe, respectively. The n-type and p-type optical surfaces are considered as ideal surface with antireflection coating during the numerical simulations.

In addition to the optical generation rate model [in (10)], the carrier generation-recombination process consists of Shockley–Read–Hall, Auger, and radiative recombination terms. The equations are [29], [31]–[35]

$$R^{\mathrm{SRH}} = A(np - n_i^2) \tag{12}$$

$$R^{\mathrm{Auger}} = (C_n n + C_p p)(np - n_i^2) \tag{13}$$

$$R^{\mathrm{Rad}} = B(np - n_i^2) \tag{14}$$

where A is the SRH recombination coefficient, C_n and C_p are the Auger recombination coefficients, and B is the radiative recombination coefficient for HgCdTe-based infrared detectors. SRH recombination can be controlled by improving the fabrication procedure among these three processes. The other two recombinations prevail in narrow bandgap photovoltaic detectors. Furthermore, Auger recombination becomes more dominant as the temperature increases and becomes crucial near room temperature. It is understood that the Auger mechanism is most likely to impose the fundamental limit to the performance of photovoltaic detectors [1], [2], [31], [32]. The extended formulae for the coefficients of A, Cn, Cp, and B in (12)–(14) can be found in [34]. Additionally, tunneling effects, such as band-to-band and trap-assisted tunneling models, are included during the simulations [7], [34], [35]. Fermi–Dirac statistics are used in the simulations with the density of states (N_c) as another tunable parameter [11].

IV. Results and Discussions

Fig. 2 shows the experimentally measured laser-irradiance-dependent LBIC signal profiles at a temperature of 120 K. The laser irradiance is increased from 1.0×10^2 to 1.0×10^5 W/cm^2. The LBIC current is measured at one contact (designated "right"), while the other contact (designated "left") is grounded. The same measurement configuration is used during the numerical simulations. Therefore, the LBIC current flowing into the "right" contact from the outside circuit is designated as the direction of positive current flow. A typical n$^+$-on-p LBIC curve is obtained with the junction width of 60 μm in the n region. The original ion implanted region is 50 μm for the n region. The increased junction width is due to the Hg interstitial diffusion [14]. There is no indication of an induced junction in the implantation region when the laser irradiance is less than 2.5×10^4 W/cm^2, as shown in Fig. 2. In the same figure, the red arrow indicates the disappearance of the LBIC peak with decreasing laser irradiance. The experiment can be repeated many times with different irradiance levels indicating that no damage to the HgCdTe device occurs. As the laser irradiance is increased to 5.0×10^4 W/cm^2, a temporary feature is created by the very high carrier injection rate from the laser. A new junction-induced LBIC with inverse polarity can be observed. It can be seen that the peak intensity is much higher than that of the original junction-induced LBIC when the laser intensity is increased to 1.0×10^5 W/cm^2. These results indicate that the induced junction is very strong at this temperature. Additionally, to illustrate the effect of the laser irradiance on the device, the net LBIC value is plotted in Fig. 3(c) by subtracting the y-axis value of Fig. 3(a) with the y-axis value of Fig. 3(b) resulting in the distinct p-n junction characteristic LBIC polarity change. So it can be inferred that there must be a new junction overlying the original junction structure.

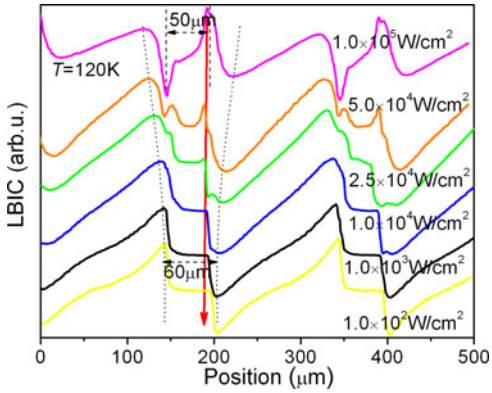

Fig. 2. Experimentally measured LBIC signal profiles (a) at a temperature of 120 K with the laser irradiances of 1.0×10^2–1.0×10^5 W/cm^2. The illumination laser wavelength is 0.63 μm.

Fig. 4 shows experimentally measured laser-irradiance-dependent LBIC signal profiles at a temperature of 300 K. The inset of Fig. 4 shows the peak-to-peak value of LBIC at different laser irradiances. It is found that the LBIC signals have significant changes at the room temperature. First, the polarity of LBIC image is reversed. It can be inferred that the configuration of the junction is very different from that at the low temperature. Second, the laser-irradiance-dependent LBIC signal profiles show a linear increase as the laser irradiances increase. At the same laser irradiance, the specific intensity of LIBC is smaller than that at low temperatures, meaning that a weaker junction is

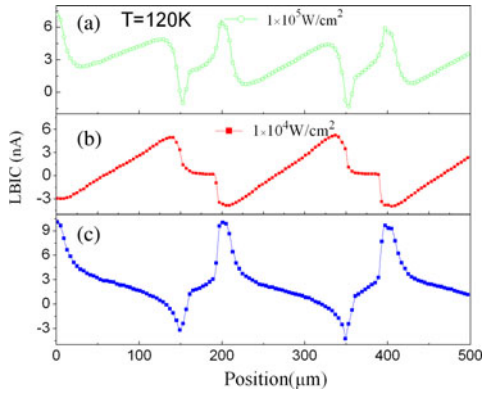

Fig. 3. Experimentally measured LBIC signal profiles (a) at a laser irradiance of 1×10^5 W/cm^2 and (b) at a laser irradiance of 1×10^4 W/cm^2. (c) Net LBIC value by subtracting the y-axis value of (a) with the y-axis value of (b). The temperature for all the measurements is 120 K.

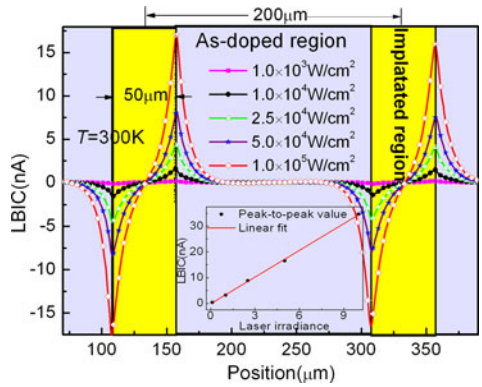

Fig. 4. Experimentally measured laser-irradiance-dependent LBIC signal profiles at a temperature of 300 K. The inset shows the peak-to-peak value of LBIC at different laser irradiances.

formed after the junction transformations at high temperatures. It can also be noticed that the LBIC signal in the ion implanted region is quite large indicating the minority carrier lifetime is comparatively longer than that at low temperatures. The type of minority carriers could possibly be changed. The above conclusions will be discussed in the following modeling and numerical simulations.

In order to understand mechanisms of the novel effects of LBIC at different laser irradiances, an ion-implantation-induced junction transformation model is proposed. The ion implantation-induced junction transformation is discussed as follows: 1) at a low temperature and a high laser irradiance as shown in Fig. 2, corresponding to the proposed model in Fig. 5(a); 2) at a low temperature and a low laser irradiance also as shown in Fig. 2; 3) at a low temperature as shown in Fig. 4, corresponding to the proposed model in Fig. 5(b).

Fig. 5 shows the schematic of the proposed ion-implantation-induced junction transformation. At low temperature and high laser irradiance, the p-n-on-p junction is formed, as shown in Fig. 5(a). Compared to temperature-induced carriers, the photo-generated carriers are in the stage of large injections. The ion implantation displaces the inner electrons causing the implanted region to consist of positively charged atomic nuclei (traps).

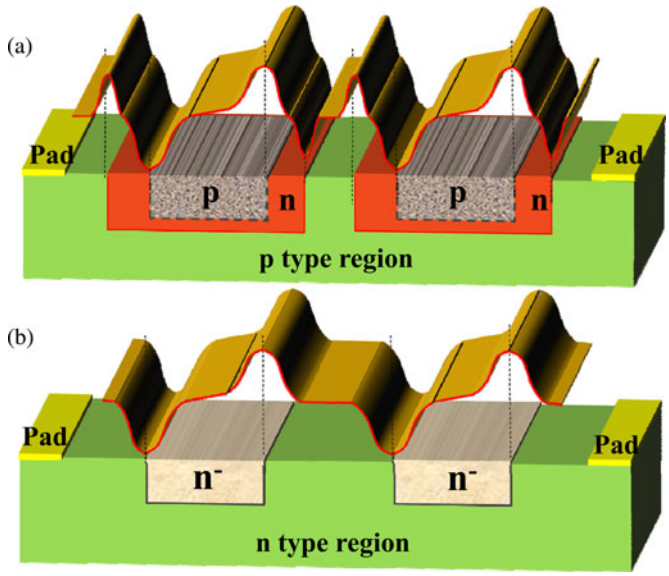

Fig. 5. Schematic of proposed ion-implantation-induced junction transformation models. (a) The p-n-on-p junction is formed at low temperature and high laser irradiance, where the photo-generated carriers are the large injection compared to temperature-induced carriers. (b) The p-on-n junction is formed at room temperature and low laser irradiance, where the photo-generated carriers are the low-level injection compared to temperature-induced carriers.

There are almost no mobile carriers in the implanted region. Several groups [36]–[38], using deep-level transient spectroscopy as well as dark current fitting [7], [11], [39], have reported that the damage from the ion implantation doping can introduce significant deep level traps in HgCdTe. A large number of traps induced by ion implantation damage in the implanted region may trap the photo-generated carriers. The type of the net traps (acceptor traps or donor traps) makes the key effect on the final junction type in the implanted region. It is well known that acceptor traps can be either negative or neutral like the acceptor. Acceptor traps are neutral when empty and negatively charged (ionized) when filled with electrons. Filled acceptor traps can emit electrons or capture holes called de-trapping. Empty acceptor traps can capture electrons or emit holes called trapping. Here, it is assumed that a large number of net bulk acceptor traps induced by damage of the ion implantation in the implanted region have trapped all of the photo-generated electrons. So the implanted region has a large number of mobile holes showing the p-type. The broaden region that shows the n-type is due to the Hg interstitial diffusion [13]. Therefore, a p-n-on-p junction is formed. The proposed model is verified by the numerical simulations, as shown in Fig. 6(a).

However, at a low temperature and low laser irradiance, the typical n-on-p junction is formed. Both the temperature-induced carriers and the photo-generated carriers are approximately equal with a low-level of incident light (low-level injections). Similarly, the acceptor traps induced by ion implantation caused damage trap all of the photo-generated electrons leaving the holes to be the mobile carriers. However, the photo-generated carrier density has decreased by two orders of magnitude compared to the case of a high level of incident light. The acceptor density (photo-generated holes) is comparable to the donor

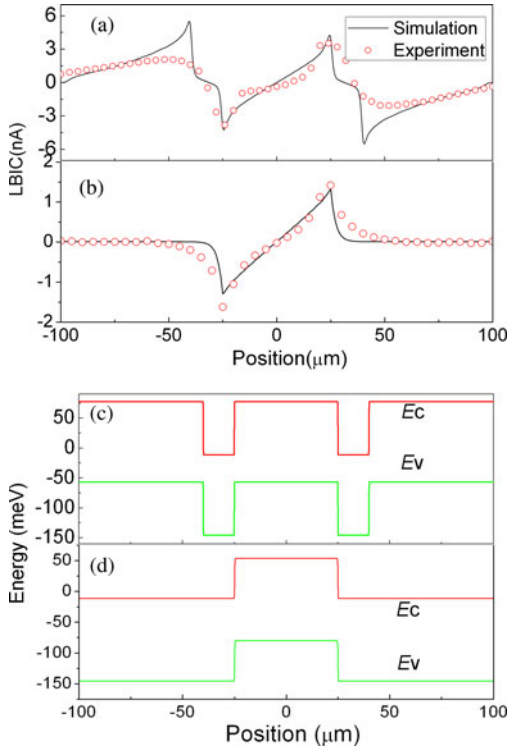

Fig. 6. Numerical simulations of the LBIC based on the proposed implantation-damage-induced junction transformation models. The dotted lines represent the experimental data. (a) The p-n-on-p junction is used at low temperature and high laser irradiance, where the photo-generated carriers are the large injection compared to temperature-induced carriers. (b) The p-on-n junction is used at room temperature and low laser irradiance, where the photo-generated carriers are the low-level injection comparing to temperature-induced carriers. (c) Equilibrium band structure of the p-n-on-p junction. (d) Equilibrium band structures of the p-on-n junction. The band profiles are cut at the junction depth of 0.5 μm along the A–B direction, as shown in Fig. 1.

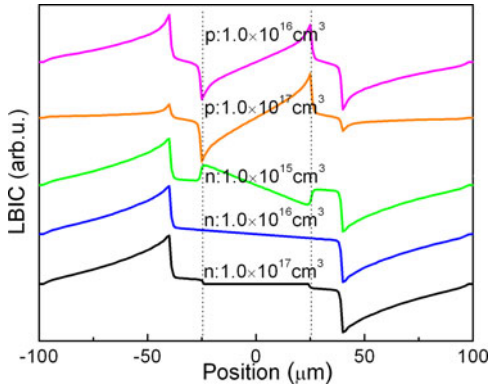

Fig. 7. Numerical simulations of the LBICs based on the proposed model in Fig. 5(a) with the different doping densities and doping types in the ion implantation region.

density from the Hg interstitial diffusion. The equilibrium Fermi level remains uniform in the implanted region. Therefore, the implanted region shows the n-type property (similar to an intrinsic semiconductor). No apparent junction is excited by the laser irradiance inside the ion implanted region. In Fig. 2, note that the LBIC at low laser irradiance is very small between the nearest two polarities, confirming that there are few mobile carriers in the implanted region.

However, at a high temperature, the p-on-n junction is formed. At near room temperatures, a relatively weak LBIC signal is induced by the p-on-n junction shown by comparing the corresponding LBIC signals of Figs. 3 and 4. When the temperature is relatively high, the density of the intrinsic carriers is possibly larger than the doping density. The mixed conduction of HgCdTe due to the temperature-generated large numbers of intrinsic carriers makes the p-type absorption layer transform to an n-type layer [40]. Therefore, the As-doped absorption layer is n-type at the room temperature. At the same time, in the implanted region, the acceptor-type traps induced by the ion implantation damage are fully activated and can trap significant numbers of free electrons. The quasi Fermi level in the implanted region is decreased, making the implanted region p-type. Note that the number of intrinsic excitations due to the high temperature is also very large in the implanted region, so the implanted region would possibly be the weak n-type. That means both p-on-n and n^--on-n are possible for the pixel array at the high temperature depending on the laser irradiance. The schematic of the p-on-n junction is shown in Fig. 5(b).

Fig. 6 shows the numerical simulation of LBICs and equilibrium band structures based on the proposed ion-implantation-induced junction transformation models. To fit the experimental LBIC signal at low temperatures and high laser irradiance, the net acceptor-type traps (bulk traps) are defined to be $2 \times 10^{16} \sim 4 \times 10^{16}$ cm^{-3} with the fixed mid-gap energy level according to the proposed model. In Fig. 3(b), in order to fit the LBIC curve at low temperature and low laser irradiance, the minority life time in the n region is very short ($\sim$0.01 ns). It is indicated that the diffusion length is very small in the ion implantation region. This is because the implantation region induces deep level traps as well as deep-level recombination centers. The experimental result of this phenomenon is also observed in Fig. 2 for laser irradiation from 1×10^2 to 2.5×10^4 W/cm^2. However, it should be noted that, at room temperature, both the experimental results and simulations show that the LBIC currents in the implantation region are larger than that at low temperatures. It appears that the junctions are completely transformed from n-on-p to p-on-n, in which the minority carriers are the electrons in the implantation region. Because the diffusion length of an electron is significantly larger than that of a hole for HgCdTe materials, the LBIC signals reflect the junction transformation demonstrating the validity of proposed models.

Further numerical simulations confirm that doping density and doping type have a significant effect on the LBICs in the ion implantation region, as shown in Fig. 7. Based on the proposed model in Fig. 5(a), a decrease of acceptor density in the implantation region can improve LBIC value of the new laser-irradiance related junction, shifting the relative LBIC value between the new junction and the original junction. When the doping type is changed to donor type in the ion implantation region, the whole LBIC signal shows the junction property at low temperature and low laser irradiance (see Fig. 2).

V. Conclusion

In conclusion, the work described in this paper provides the basic mechanisms for a better understanding of junction transformation for long wavelength HgCdTe infrared detector pixel arrays. The model for ion-implantation-induced junction transformations is developed and numerically demonstrated to analyze the novel characteristics of LBICs. The results show that Hg interstitial diffusion and ion implantation damage are key factors in inducing the LBIC coupling, polarity reversion, and junction broadening at different laser irradiances. The trap density of approximately $2 \times 10^{16} \sim 4 \times 10^{16}$ cm^{-3} with the fixed mid-gap energy level in the ion implantation damage region is obtained by using numerical simulations. Furthermore, when the number of temperature-induced intrinsic carriers for long wavelength material is comparable to that of the doping intensity and photo-generated carriers, the behavior of temperature-induced intrinsic carriers is another key factor that determines the tradeoff of junction transitions. This work provides a method to judge the change of LBIC when it is used on HgCdTe infrared photovoltaic detector array pixels, as well as for junction characterization of a near room temperature operating photodetector.

Acknowledgment

The authors appreciate J. Torley from the University of Colorado at Colorado Springs for critical reading of the manuscript.

References

[1] A. Rogalski, J. Antoszewski, and L. Faraone, "Third-generation infrared photodetector arrays," *J. Appl. Phys.*, vol. 105, pp. 091101-1–091101-3, 2009.

[2] P. Norton, "HgCdTe infrared detectors," *Opto-Electron. Rev.*, vol. 10, pp. 159–174, 2002.

[3] J. Wang, X. S. Chen, W. D. Hu, L. Wang, W. Lu, F. Q. Xu, J. Zhao, Y. L Shi, and R. B. Ji, "Amorphous HgCdTe infrared photoconductive detector with high detectivity above 200 K," *Appl. Phys. Lett.*, vol. 99, pp. 113508-1–113508-3, 2011.

[4] A. Rogalski, "HgCdTe infrared detector material: History, status and outlook," *Rep. Prog. Phys.*, vol. 68, pp. 2267–2336, 2005.

[5] W. D. Hu, X. S. Chen, Z. H. Ye, and W. Lu, "A hybrid surface passivation on HgCdTe long wave infrared detector with in-situ CdTe deposition and high-density Hydrogen plasma modification," *Appl. Phys. Lett.*, vol. 99, pp. 091101-1–091101-3, 2011.

[6] F. X. Zha, S. M. Zhou, H. L. Ma, F. Yin, B. Zhang, T. X. Li, J. Shao, and X. C. Shen, "Laser drilling induced electrical type inversion in vacancy-doped p-type HgCdTe," *Appl. Phys. Lett.*, vol. 93, pp. 151113-1–151113-3, 2008.

[7] W. D. Hu, X. S. Chen, F. Yin, Z. J. Quan, Z. H. Ye, X. N. Hu, Z. F. Li, and W. Lu, "Analysis of temperature dependence of dark current mechanisms for long-wavelength HgCdTe photovoltaic infrared detectors," *J. Appl. Phys.*, vol. 105, pp. 104502-1–104502-8, 2009.

[8] F. Y. Yue, J. H. Chu, J. Wu, Z. G. Hu, Y. W. Li, and P. X. Yang, "Modulated photoluminescence of shallow levels in arsenic-doped $Hg_{1-x}Cd_xTe$ ($x \approx 0.3$) grown by molecular beam epitaxy," *Appl. Phys. Lett.*, vol. 92, pp. 121916-1–121916-3, 2008.

[9] K. Jóźwikowski, M. Kopytko, A. Rogalski, and A. Jóźwikowska, "Enhanced numerical analysis of current-voltage characteristics of long wavelength infrared n-on-p HgCdTe photodiodes," *J. Appl. Phys.*, vol. 108, pp. 074519-1–074519-11, 2010.

[10] F. Y. Yue, J. Wu, and J. H. Chu, "Deep/shallow levels in arsenic-doped HgCdTe determined by modulated photoluminescence spectra," *Appl. Phys. Lett.*, vol. 93, pp. 131909-1–131909-3, 2008.

[11] W. D. Hu, X. S. Chen, Z. H. Ye, J. Zhang, F. Yin, C. Lin, Z. F. Li, and W. Lu, "Accurate simulation of temperature dependence of dark current in HgCdTe infrared detector assisted by analytical modeling," *J. Electron. Mater.*, vol. 39, pp. 981–985, 2010.

[12] Challenges for the ITRS. 2013. [Online]. Available: http://www.itrs.net

[13] L. O. Bubulac and W. E. Tennant, "Role of Hg in junction formation in ion-implanted HgCdTe," *Appl. Phys. Lett.*, vol. 51, pp. 355–357, 1987.

[14] W. D. Hu, X. S. Chen, Z. H. Ye, Y. G. Chen, F. Yin, B. Zhang, and W. Lu, "Polarity inversion and coupling of laser beam induced current in As-doped long-wavelength HgCdTe infrared detector pixel arrays: Experiment and simulation," *Appl. Phys. Lett.*, vol. 101, pp. 181108-1–181108-5, 2012.

[15] D. A. Redfern, C. A. Musca, J. M. Dell, and L. Faraone, "Characterization of electrically active defects in photovoltaic detector arrays using laser beam-induced current," *IEEE Trans. Electron Devices*, vol. 52, no. 10, pp. 2163–2174, Oct. 2005.

[16] D. A. Redfern, W. Fang, K. Ito, G. Bahir, C. A. Musca, J. M. Dell, and L. Faraone, "Investigation of laser beam-induced current techniques for heterojunction photodiode characterization," *J. Appl. Phys.*, vol. 98, pp. 034501-1–034501-9, 2005.

[17] F. Yin, W. D. Hu, B. Zhang, Z. F. Li, X. N. Hu, X. S. Chen, and W. Lu, "Simulation of laser beam induced current for HgCdTe photodiodes with leakage current," *Opt. Quantum Electron.*, vol. 41, pp. 805–810, 2009.

[18] F. X. Zha, M. S. Li, J. Shao, W. T. Yin, S. M. Zhou, X. Lu, Q. T. Guo, Z. H. Ye, T. X. Li, H. L. Ma, B. Zhang, and X. C. Shen, "Femtosecond laser-drilling-induced HgCdTe photodiodes," *Opt. Lett.*, vol. 35, pp. 971–973, 2010.

[19] D. A. Redfern, E. P. G. Smith, C. A. Musca, J. M. Dell, and L. Faraone, "Interpretation of current flow in photodiode structures using laser beam-induced current for characterization and diagnostics," *IEEE Trans. Electron Devices*, vol. 53, no. 1, pp. 23–31, Jan. 2006.

[20] W. Fang, K. Ito, and D. A. Redfern, "Parameter identification for semiconductor diodes by LBIC imaging," *SIAM J. Appl. Math.*, vol. 62, pp. 2149–2174, 2002.

[21] D. A. Redfern, W. Fang, K. Ito, C. A. Musca, J. M. Dell, and L. Faraone, "Low temperature saturation of p–n junction laser beam induced current signals," *Solid-State Electron.*, vol. 48, pp. 409–414, 2004.

[22] D. A. Redfern, C. A. Musca, J. M. Dell, and L. Faraone, "Correlation of laser-beam-induced current with current-voltage measurements in HgCdTe photodiodes," *J. Electron. Mater.*, vol. 33, pp. 560–571, 2004.

[23] L. O. Bubulac, "Dependence of junction formation on substrate in implanted HgCdTe," *Appl. Phys. Lett.*, vol. 46, pp. 976–978, 1985.

[24] A. Jozwikowska, K. Jozwikowski, J. Antoszewski, C. A. Musca, T. Nguyen, R. H. Sewell, J. M. Dell, L. Faraone, and Z. Orman, "Generation-recombination effects on dark currents in CdTe-passivated midwave infrared HgCdTe photodiodes," *J. Appl. Phys.*, vol. 98, pp. 014504-1–014504-11, 2005.

[25] W. D. Hu, X. S. Chen, F. Yin, Z. H. Ye, C. Lin, X. N. Hu, Z. J. Quan, Z. F. Li, and W. Lu, "Simulation and design consideration of photoresponse for HgCdTe infrared photodiodes," *Opt. Quantum Electron.*, vol. 40, pp. 1255–1260, 2008.

[26] J. P. Rosbeck, R. E. Star, S. L. Price, and K. J. Riley, "Background and temperature dependent current–voltage characteristics of $Hg_{1-x}Cd_xTe$ photodiodes," *J. Appl. Phys.*, vol. 53, pp. 6430–6440, 1982.

[27] N. Guo, W. D. Hu, X. S. Chen, C. Meng, Y. Q. Lv, and W. Lu, "Optimization of microlenses for InSb infrared focal-plane arrays," *J. Electron. Mater.*, vol. 40, pp. 1647–1650, 2011.

[28] W. D. Hu, X. S. Chen, Z. H. Ye, and W. Lu, "An improvement on short-wavelength photoresponse for a heterostructure HgCdTe two-color infrared detector," *Semicond. Sci. Technol.*, vol. 25, pp. 045028-1–045028-5, 2010.

[29] E. Bellotti and D. D. Orsogna, "Numerical analysis of HgCdTe simultaneous two-color photovoltaic infrared detectors," *IEEE J. Quantum Electron.*, vol. 42, no. 4, pp. 418–426, Apr. 2006.

[30] J. Wenus, J. Rutkowski, and A. Rogalski, "2D analysis of double layer heterojunction HgCdTe photodiodes," *IEEE Trans. Electron Devices*, vol. 48, no. 7, pp. 1326–1332, Jul. 2001.

[31] D. D'Orsogna, S. Tobin, and E. Bellotti, "Numerical analysis of a very long-wavelength HgCdTe pixel array for infrared detection," *J. Electron. Mater.*, vol. 37, pp. 1349–1355, 2008.

[32] C. A. Keasler, M. Moresco, D. D'Orsogna, P. Lamrre, and E. Bellotti, "3D numerical analysis of As-diffused HgCdTe planar pixel arrays," *Proc. SPIE*, vol. 7780, pp. 77800J-1–77800J-6, 2010.

[33] C. A. Keasler and E. Bellotti, "Three-dimensional electromagnetic and electrical simulation of HgCdTe pixel arrays," *J. Electron. Mater.*, vol. 40, pp. 1795–1801, 2011.

[34] H. Kocer, Y. Arslan, and C. Besikci, "Numerical analysis of long wavelength infrared HgCdTe photodiodes," *Infrared Phys. Technol.*, vol. 55, pp. 49–55, 2012.

[35] H. Kocer, "Numerical device simulation to investigate the noise currents of mercury cadmium telluride photosensors for thermal imaging applications," *Int. J. Numer. Model.*, 2013, to be published.
[36] V. I. Turinov, "A study of deep levels in CdHgTe by analyzing the tunneling current of photodiodes," *Semiconductors*, vol. 38, pp. 1092–1098, 2004.
[37] C. E. Jones, K. James, J. Merz, R. Braunstein, M. Burd, M. Eetemadi, S. Hutton, and J. Drumheller, "Status of point defects in HgCdTe," *J. Vac. Sci. Technol.*, vol. A3, pp. 131–137, 1985.
[38] D. L. Polla and C. E. Jones, "Deep level studies of $Hg_{1-x}Cd_xTe$. I: Narrow-band-gap space-charge spectroscopy," *J. Appl. Phys.*, vol. 52, pp. 5118–5131, 1981.
[39] J. V. Gumenjuk-Sichevskaja, F. F. Sizov, V. N. Ovsyuk, V. V. Vasil'ev, and D. G. Esaev, "Charge transport in HgCdTe-based n+-p photodiodes," *Semiconductors*, vol. 35, pp. 800–806, 2001.
[40] S. E. Schacham and E. Finkman, "Light modulated hall effect for extending characterization of semiconductor materials," *J. Appl. Phys.*, vol. 60, pp. 2860–2865, 1986.

Wei-Da Hu received the B.S. and M.S. degrees in material science from the Wuhan University of Technology, Wuhan, China, in 2001 and 2004, respectively, and the Ph.D. degree (with Hons.) in microelectronics and solid-state electronics from the Shanghai Institute of Technology Physics, Chinese Academy of Sciences, Shanghai, China, in 2007.

His experiences range from HgCdTe-based photodetector simulations to GaN-based devices design and simulations. He is currently an Associate Professor on modeling, simulation, and design of photodetectors at the Shanghai Institute of Technology Physics, Shanghai, China. His current research interests include simulation and modeling of infrared photodetector, fabrication and characterization of nano-photodetector based on Nano-MOFETs, and device physics of GaN-based photodetectors.

Dr. Hu has authored or coauthored more than 50 peer-reviewed journal publications. He is the Program Committee of the International Conference on Numerical Simulation of Optoelectronic Devices.

Xiao-Shuang Chen received the Ph.D. degree in condensed matter physics from Nanjing University, Jiangsu, China, in 1995.

His current research interests include infrared photo-electronic material design, high speed electronic device design, and photonic crystals. He has been a Research Fellow at the Korea Institute of Advanced Study, University of Tokyo, Japan, and Humboldt Research Fellow at Universität Würzburg, Germany. He has coauthored more than 150 publications. He is currently a Professor at the Shanghai Institute of Technology Physics, and the Director of the National Laboratory for Infrared Physics.

Prof. Chen has won many national prizes for solving problems in infrared electronics.

Zhen-Hua Ye received the Ph.D. degree in microelectronics and solid-state electronics from the Shanghai Institute of Technical Physics, Chinese Academy of Sciences, Shanghai, China.

His current research interests include optimization, processing, and fabrication of HgCdTe-based photodetectors.

A-Li Feng is currently working toward the M.S. degree in microelectronics and solid-state electronics at the Shanghai Institute of Technical Physics, Chinese Academy of Sciences, Shanghai, China.

Her current research interests include simulation and modeling of HgCdTe-based photodetectors.

Fei Yin received the Ph.D. degree in microelectronics and solid-state electronics from the Shanghai Institute of Technical Physics, Chinese Academy of Sciences, Shanghai, China.

Her current research interests include optimization, modeling of HgCdTe-based photodetectors, and COMS devices.

Bo Zhang received the Ph.D. degree in physics from Tongji University, Shanghai, China. He is currently a Professor at the Shanghai Institute of Technology Physics, Chinese Academy of Sciences, Shanghai.

His current research interest includes optical characterization of photodetectors.

Lei Liao was born in Hubei, China, in 1981. From 2000 to 2009, he studied at Wuhan University, Hubei, where he received the B.S. and Ph.D. degrees, both in materials science and engineering. From 2009 to 2011, he was a Postdoctoral Researcher in Prof. Xiangfeng Duan's Group, Department of Chemistry and Biochemistry, University of California Los Angeles.

Prof. Liao has coauthored more than 60 peer-reviewed journal publications in the area of nanomaterials and nanoelectronics, with about more than 2200 citations. His current research interests include nanomaterials and nanoelectronics.

Wei Lu received the B.S. degree in physics from Fudan University, Shanghai, China, in 1983, and the Ph.D. degree from the Shanghai Institute of Technology Physics, Chinese Academy of Sciences, Shanghai, in 1988. Since 1989, he has been a Research Fellow at the Technical University of Braunschweig, Germany, and a Visiting Professor in many countries. He is currently a Professor at the Shanghai Institute of Technology Physics, and the Director of the National Laboratory for Infrared Physics and Shanghai Physical Society. He has authored or coauthored more than 150 publications on optoelectronic materials and devices. His current research interests include HgCdTe-based photodetectors, semiconductor physics, solid spectroscopy, and condensed matter physics.

Prof. Lu has received many national awards and serves on the editorial board of the *Journal of Applied Physics*.